

Post-Newtonian analysis of precessing convention for spinning compact binaries

A Gupta^{1,2} and A Gopakumar¹

¹Department of Astronomy and Astrophysics, Tata Institute of Fundamental Research, Mumbai 400005, India

²Inter University Centre for Astronomy and Astrophysics, Ganeshkhind, Pune 411007, India

E-mail: anuradha@iucaa.ernet.in, gopu@tifr.res.in

Abstract. A precessing source frame, constructed using the Newtonian orbital angular momentum \mathbf{L}_N , can be invoked to model inspiral gravitational waves from generic spinning compact binaries. An attractive feature of such a precessing convention is its ability to remove all spin precession induced modulations from the orbital phase evolution. However, this convention usually employs a post-Newtonian (PN) accurate precessional equation, appropriate for the PN accurate orbital angular momentum \mathbf{L} , to evolve the \mathbf{L}_N -based precessing source frame. This influenced us to develop inspiral waveforms for spinning compact binaries in a precessing convention that explicitly employ \mathbf{L} to describe the binary orbits. Our approach introduces certain additional 3PN order terms in the evolution equations for the orbital phase and frequency with respect to the usual \mathbf{L}_N -based implementation of the precessing convention. We examine the practical implications of these additional terms by computing the match between inspiral waveforms that employ \mathbf{L} and \mathbf{L}_N -based precessing conventions. The match estimates are found to be smaller than the optimal value, namely 0.97, for a non-negligible fraction of unequal mass spinning compact binaries.

PACS numbers: 04.25.Nx, 04.30.-w, 97.60.Lf, 95.30.Sf

Submitted to: *Class. Quantum Grav.*

1. Introduction

Inspiralling compact binaries containing spinning neutron stars and (or) black holes (BHs) are key sources for the network of second generation interferometric gravitational wave (GW) detectors [1]. These instruments include the two advanced LIGO (aLIGO) observatories [2], the advanced Virgo [3], the KAGRA [4], the GEO-HF [5] and the planned LIGO-India [6]. In contrast, massive spinning BH binaries are one of the most exciting sources for the space-based GW observatory like the planned eLISA [7]. GWs from such inspiralling compact binaries, whose components are specified by their masses and spins, can be accurately modeled using perturbative approaches to tackle the underlying Einstein field equations [8]. Therefore, the optimal detection technique of *matched filtering* can be employed to detect and characterize inspiral GWs from such binaries [9, 10]. This involves cross correlating

the interferometric output data with a bank of templates that theoretically model inspiral GWs from spinning compact binaries. A successful detection demands that at least one template should remain in phase as much as possible with the buried weak GW signals in the frequency windows of various GW observatories [11].

During the GW emission induced inspiral, dynamics and associated GWs from compact binaries can be accurately described using the post-Newtonian (PN) approximation to general relativity [8, 12]. The PN description provides interesting quantities, required for various template constructions, as an asymptotic series in terms of certain dimensionless parameter. For binaries in quasi-circular orbits, it is usual to use $x = (Gm\omega/c^3)^{2/3}$ as the PN expansion parameter while constructing inspiral templates, where m and ω stand for the total mass and orbital (angular) frequency of the binary [13, 14]. Currently, GW frequency and associated phase evolution, crucial inputs to construct various inspiral template families, are known to 3.5PN order for non-spinning compact binaries [15, 16]. In other words, PN corrections to the above two quantities are computed to the $x^{7/2}$ order beyond the leading quadrupolar (Newtonian) order for such binaries. Moreover, the amplitudes of the two GW polarization states, h_{\times} and h_{+} , for non-spinning binaries are available to 3PN order [17]. Very recently, detailed computations led to the determination of the dynamics of such binaries to the 4PN order [18]. Binaries that contain compact objects with intrinsic rotations, the spin effects enter the dynamics and GW emission via spin-orbit and spin-spin interactions [19, 20]. In binaries containing maximally spinning BHs, the spin-orbit coupling (linear in the spins) first appears at the 1.5PN order, while the spin-spin interaction (which is quadratic in spins) first occurs at the 2PN order [21]. Additionally, \mathbf{S}_1 , \mathbf{S}_2 and \mathbf{L} , the two spin and orbital angular momenta, for generic spinning compact binaries precess around the total angular momentum $\mathbf{J} = \mathbf{L} + \mathbf{S}_1 + \mathbf{S}_2$ due to spin-orbit and spin-spin interactions. This forces substantial modulations of the emitted GWs from inspiralling generic spinning compact binaries compared to their non-spinning counterparts [21, 22]. Therefore, it is important to incorporate various effects due to the intrinsic rotations of compact objects while constructing inspiral GW templates for spinning compact binaries. At present, GW frequency evolution and amplitudes of h_{\times} and h_{+} for BH binaries having maximally spinning components are fully determined to 2.5PN and 2PN orders, respectively, while incorporating all the relevant spin induced effects [21, 23, 24, 25, 26, 27]. Moreover, the on-going detailed computations are providing various higher PN order spin-orbit and spin-spin contributions to the dynamics of spinning compact binaries in general orbits and to the orbital frequency evolution for quasi-circular inspiral. At present, the spin-orbit contributions to binary dynamics and GW frequency evolution are available up to the next-to-next-to-leading order (2PN order) beyond the leading order [28, 29] while adapting the MPM (Multipolar post-Minkowskian) approach [30]. In contrast, the higher order spin-spin contributions to the binary dynamics are usually tackled in the Arnowitt-Deser-Misner canonical formalism [31] and in the Effective Field Theory formalism [32, 33] (Note that the spin-orbit effects in the Effective Field Theory formalism are computed, for example, in [34]). These approaches provide various spin(1)-spin(2) and spin-squared contributions to the orbital dynamics [35]. Moreover, various source multipole moments needed to obtain the spin contributions to GW luminosity at the 3PN order and GW polarization states to the 2.5PN order were computed in [36].

The construction of time-domain h_{\times} and h_{+} associated with inspiralling generic spinning compact binaries requires us to numerically solve a set of PN accurate

differential equations for $\mathbf{S}_1, \mathbf{S}_2, \mathbf{L}_N, x$ and the orbital phase [21], where \mathbf{L}_N is the Newtonian orbital angular momentum. The numerical integration provides temporal evolutions for the orbital phase, the associated angular frequency and the two angles that specify the orientation of the orbital plane in an inertial frame associated with the direction of \mathbf{J} at the initial epoch. These variations are incorporated into the PN accurate expressions for h_\times and h_+ to obtain PN accurate time-domain inspiral waveforms from such binaries [21]. In this approach, the differential equation for the orbital phase explicitly depends on the precessional motion of the orbital plane [21, 22]. Therefore, it is not possible to express the orbital phase as an integral of the orbital frequency as usually done in the case of non-spinning compact binaries [11]. A decade ago, Buonanno, Chen and Vallisneri proposed an approach, referred to as the precessing convention, that factorizes the generic spinning binary waveform into a *carrier signal* and a *modulated amplitude* term [37]. In this approach, the phase of the carrier signal (Φ_p) essentially coincides with the accumulated orbital phase such that $\dot{\Phi}_p \equiv \omega$. Moreover, the precessional dynamics of the orbital plane only influences the modulated amplitude part of inspiral waveform even for generic compact binaries. Therefore, the precessing convention disentangles the precessional effects from its non-precessional counterparts while modeling both the amplitude and the phase evolutions of inspiral GWs from such astrophysical systems. This convention was employed to model inspiral GW signals from compact binaries containing misaligned single-spin and to probe its data analysis benefits [38, 39]. Very recently, inspiral-merger-ringdown waveforms for generic spinning BH binaries, invoking the effective-one-body approach [40], also adapted the precessing convention to model GWs from the inspiral part [41]. We note that this convention requires a *precessing source frame* which is usually based on the Newtonian orbital angular momentum \mathbf{L}_N . However, [41] employed both \mathbf{L} and \mathbf{L}_N to model GWs during the late part of the binary inspiral just prior to the plunge.

In this paper, we develop a prescription to compute PN accurate inspiral waveforms for generic spinning compact binaries while using the PN accurate orbital angular momentum \mathbf{L} to construct the precessing source frame. This is influenced by the usual practice of employing precessional equation appropriate for \mathbf{L} to evolve \mathbf{L}_N and the associated precessing source frame while constructing inspiral waveforms via the precessing convention of [37]. We show that the use of such an adiabatic approximation, namely employing an orbital averaged differential equation for \mathbf{L}_N , can lead to PN corrections to $\dot{\Phi}_p = \omega$. These observations motivated us to provide a set of PN accurate equations to obtain temporally evolving quadrupolar order inspiral GW polarization states for generic spinning compact binaries in the \mathbf{L} -based precessing convention. In our approach, the spin precession induced modulations enter the differential equation for the orbital phase only at the 3PN order. Moreover, the \mathbf{L} -based convention requires us to include additional 3PN order terms in the differential equation for x , compared to the usual \mathbf{L}_N -based approach. We explore the practical implications of these additional terms with the help of *match* computations, detailed in [11, 42]. The match computations involve two inspiral families where one is constructed via our \mathbf{L} -based precessing convention and therefore incorporate the above mentioned 3PN order terms. The other family is based on the LALSUITE SpinTaylorT4 code, developed by the LIGO Scientific Collaboration (LSC) [43], that implemented the \mathbf{L}_N -based precessing convention of [37]. In this code, the precessional dynamics is fully 2PN accurate while the differential equation for x incorporates spin-orbit contributions to 3.5PN order. For match computations, we employ PN accurate

relation connecting \mathbf{L}_N and \mathbf{L} to construct two waveform families with physically identical initial orbital and spin orientations. We terminate the two inspiral waveform families when their respective x parameter reaches 0.1 which roughly corresponds to orbital separations $\sim 10 Gm/c^2$. These considerations allow us to attribute the reported match estimates to the above mentioned additional 3PN order terms present in our differential equations for the orbital phase and frequency. We find that the match estimates are less than the optimal 0.97 value for a non-negligible fraction of unequal mass spinning compact binaries. It may be recalled that such an optimal match value roughly corresponds to a 10% loss in the ideal event rate.

In what follows, we briefly summarize the usual implementation of the \mathbf{L}_N -based precessing convention and explore the consequence of employing an orbital averaged precessional equation for \mathbf{L}_N . In section 2.2, we detail the construction of quadrupolar order GW polarization states in our \mathbf{L} -based precessing convention. The match estimates involving these two inspiral families with physically equivalent initial configurations and associated discussions are listed in section 3 while section 4 provides a brief summary.

2. Inspiral waveforms in \mathbf{L}_N and \mathbf{L} -based precessing conventions

We begin by summarizing the usual implementation of the \mathbf{L}_N -based precessing convention and explore the consequence of employing an orbital averaged differential equation for \mathbf{L}_N .

2.1. The \mathbf{L}_N -based precessing convention

The precessing convention, introduced in [37], aims to remove all the spin precession induced modulations from the orbital phase evolution. In this approach, the orbital phase $\Phi_p(t)$ is written as an integral of the orbital frequency $\omega(t)$, namely $\Phi_p(t) = \int \omega(t') dt'$, even for generic spinning compact binaries. This feature is crucial to ensure that the inspiral waveform for a precessing spinning compact binary can be written as the product of a non-precessing carrier waveform and a modulation term that contains all the precessional effects. This is how the approach disentangles the precessional effects from their non-precessional counterparts both in the amplitude and phase of inspiral waveforms. It should be noted that in the absence of precessing convention, the orbital phase of a generic spinning binary is given by $\int [\omega(t') - \dot{\alpha}'(t') \cos \iota'(t')] dt'$, where ι' and α' specify the orientation of \mathbf{L}_N in an inertial frame associated with the initial direction of \mathbf{J} [21].

To obtain inspiral waveforms for spinning compact binaries in their precessing convention, [37] employed certain *precessing source frame* ($\mathbf{e}_1^l, \mathbf{e}_2^l, \mathbf{e}_3^l \equiv \mathbf{l}$), where \mathbf{l} is the unit vector along \mathbf{L}_N . The basis vectors of this triad satisfy the evolution equations $\dot{\mathbf{e}}_{1,2}^l = \boldsymbol{\Omega}_e^l \times \mathbf{e}_{1,2}^l$ and $\dot{\mathbf{e}}_3^l \equiv \dot{\mathbf{l}} = \boldsymbol{\Omega}_k \times \mathbf{l}$. The angular frequency $\boldsymbol{\Omega}_e^l$ is constructed in such a manner that these three basis vectors always form an orthonormal triad. This is possible with the following expression for $\boldsymbol{\Omega}_e^l$, namely $\boldsymbol{\Omega}_e^l = \boldsymbol{\Omega}_k - (\boldsymbol{\Omega}_k \cdot \mathbf{l})\mathbf{l}$, where $\boldsymbol{\Omega}_k$ is the usually employed precessional frequency for \mathbf{l} . The expression for $\boldsymbol{\Omega}_k$ that includes the dominant order spin-orbit and spin-spin contributions can be obtained by collecting the terms that multiply $\hat{\mathbf{L}}_N (\equiv \mathbf{l})$ in equation (9) of [37]. With the help of \mathbf{e}_1^l and \mathbf{e}_2^l , an orbital phase $\Phi_p(t)$ may be defined such that $\mathbf{n} = \cos \Phi_p \mathbf{e}_1^l + \sin \Phi_p \mathbf{e}_2^l$, where \mathbf{n} is the unit vector along the binary separation vector \mathbf{r} . Additionally, one may define a co-moving frame ($\mathbf{n}, \boldsymbol{\lambda} = \mathbf{l} \times \mathbf{n}, \mathbf{l}$) such that the time derivative of \mathbf{n} is given by

$\dot{\mathbf{n}} = \dot{\Phi}_p \boldsymbol{\lambda} + \boldsymbol{\Omega}_e^l \times \mathbf{n}$. It was argued in [37] that $\boldsymbol{\Omega}_e^l$ should only be proportional to \mathbf{n} which ensures that $\dot{\mathbf{n}} \cdot \boldsymbol{\lambda} = \dot{\Phi}_p$. This leads to the desirable expression for $\dot{\Phi}_p$, namely $\dot{\Phi}_p = \omega$, while employing the adiabatic condition for the sequence of circular orbits: $\dot{\mathbf{n}} \cdot \boldsymbol{\lambda} = \omega$. This adiabatic condition is equivalent to $\dot{\mathbf{n}} \cdot \dot{\mathbf{n}} \equiv \omega^2$ that provides another version of the PN independent relation connecting the linear and orbital angular velocities, $v^2 \equiv r^2 \omega^2$.

A close inspection reveals that this approach usually employs an orbital averaged differential equation for \mathbf{L}_N to evolve the precessing source frame while constructing PN accurate inspiral waveforms. It turns out that the differential equation for \mathbf{L}_N in such an adiabatic approximation is identical to the evolution equation for the PN accurate orbital angular momentum \mathbf{L} [44, 45]. In what follows, we explore the effect of such an adiabatic approximation on the equation for $\dot{\mathbf{n}}$ in the $(\mathbf{n}, \boldsymbol{\lambda}, \mathbf{l})$ co-moving frame and on the derivation of $\dot{\Phi}_p$ equation. The usually employed expression for $\boldsymbol{\Omega}_k$ while considering only the leading order spin-orbit interactions may be written as

$$\boldsymbol{\Omega}_k = \frac{c^3}{Gm} x^3 \left\{ \delta_1 q \chi_1 \mathbf{s}_1 + \frac{\delta_2}{q} \chi_2 \mathbf{s}_2 \right\}, \quad (1)$$

where $q = m_1/m_2$ ($m_1 \geq m_2$) is the mass ratio and $\delta_{1,2} = \eta/2 + 3(1 \mp \sqrt{1-4\eta})/4$ while $\eta = m_1 m_2/m^2$ is the symmetric mass ratio. The Kerr parameters χ_1 and χ_2 of the two compact objects of mass m_1 and m_2 specify their spin angular momenta by $\mathbf{S}_{1,2} = G m_{1,2}^2 \chi_{1,2} \mathbf{s}_{1,2}/c$, where \mathbf{s}_1 and \mathbf{s}_2 are the unit vectors along \mathbf{S}_1 and \mathbf{S}_2 . It is straightforward to show that the above equation is identical to ω^2 terms that multiply $\hat{\mathbf{L}}_N$ on the right hand side of equation (9) in [37]. To explore the implication of using the above expression for $\boldsymbol{\Omega}_k$ to construct $\boldsymbol{\Omega}_e^l$, we revisit the arguments detailed in the appendix B of [37]. These arguments, crucial to obtain $\dot{\Phi}_p = \omega$, require that $\boldsymbol{\Omega}_e^l \times \mathbf{n}$, appearing in the equation $\dot{\mathbf{n}} = \dot{\Phi}_p \boldsymbol{\lambda} + \boldsymbol{\Omega}_e^l \times \mathbf{n}$, should be zero. A closer look reveals that [37] did not use the explicit expression for $\boldsymbol{\Omega}_e^l$ to show that $\boldsymbol{\Omega}_e^l$ lies along \mathbf{n} . Instead, the authors arrived at such a conclusion with the help of the following two steps. First, it was noted that $\dot{\mathbf{l}}$ should be $\propto \boldsymbol{\lambda}$ (see lines around equations (B3), (B4) and (B5) in [37]). This was inferred by employing the definition for \mathbf{l} ($\mathbf{l} = \mathbf{n} \times \boldsymbol{\lambda}$), the resulting time derivative for \mathbf{l} ($\dot{\mathbf{l}} = \dot{\mathbf{n}} \times \boldsymbol{\lambda} + \mathbf{n} \times \dot{\boldsymbol{\lambda}}$), the adiabatic condition for circular orbits ($\dot{\mathbf{n}} = \omega \boldsymbol{\lambda}$) and the time derivative for $\boldsymbol{\lambda}$ in the co-moving frame ($\dot{\boldsymbol{\lambda}} = -\dot{\Phi}_p \mathbf{n} + \boldsymbol{\Omega}_e^l \times \boldsymbol{\lambda}$). In the second step, [37] invoked the requirement that $\dot{\mathbf{l}}$ should also be given by $\boldsymbol{\Omega}_e^l \times \mathbf{l}$ in the precessing source frame. With the help of the above two arguments, namely $\dot{\mathbf{l}} \propto \boldsymbol{\lambda}$ and $\dot{\mathbf{l}} = \boldsymbol{\Omega}_e^l \times \mathbf{l}$, [37] concluded that $\boldsymbol{\Omega}_e^l$ should lie along \mathbf{n} as $\boldsymbol{\lambda} = \mathbf{l} \times \mathbf{n}$. We would like to emphasize that [37] never invoked their explicit expression for $\boldsymbol{\Omega}_e^l$ to show that $\boldsymbol{\Omega}_e^l$ can have components only along \mathbf{n} which is essential to obtain the relation $\dot{\Phi}_p = \omega$. In fact, it is straightforward to show with the help of equation (1) that $\boldsymbol{\Omega}_e^l$ can have components along $\boldsymbol{\lambda}$ since $\boldsymbol{\Omega}_e^l \cdot \boldsymbol{\lambda} = (c^3/Gm) x^3 (\delta_1 q \chi_1 \mathbf{s}_1 \cdot \boldsymbol{\lambda} + \delta_2 \chi_2/q \mathbf{s}_2 \cdot \boldsymbol{\lambda}) \neq 0$, in general. This results in the following 1.5PN accurate expression for $\dot{\mathbf{n}}$

$$\dot{\mathbf{n}} = \dot{\Phi}_p \boldsymbol{\lambda} + \frac{c^3}{Gm} x^3 \left\{ \delta_1 q \chi_1 [\mathbf{s}_1 \times \mathbf{n} - (\mathbf{s}_1 \cdot \mathbf{l}) \boldsymbol{\lambda}] + \frac{\delta_2}{q} \chi_2 [\mathbf{s}_2 \times \mathbf{n} - (\mathbf{s}_2 \cdot \mathbf{l}) \boldsymbol{\lambda}] \right\}. \quad (2)$$

Clearly, the 1.5PN order terms that arise from $\boldsymbol{\Omega}_e^l \times \mathbf{n}$ in the above equation will not be zero for generic spinning compact binaries.

Interestingly, it is still possible to equate $\dot{\Phi}_p$ to ω by employing the adiabatic condition $\dot{\mathbf{n}} \cdot \boldsymbol{\lambda} = \omega$ as $(\boldsymbol{\Omega}_e^l \times \mathbf{n}) \cdot \boldsymbol{\lambda} = 0$ even in the presence of non-vanishing 1.5PN

order $\Omega_e^l \times \mathbf{n}$ term. However, the equivalent version of the adiabatic condition, namely $\dot{\mathbf{n}} \cdot \dot{\mathbf{n}} \equiv \omega^2$, forces the differential equation for Φ_p to contain 3PN order corrections in addition to the standard ω term. In other words, two equivalent versions of the same adiabatic condition for circular orbits, namely $\dot{\mathbf{n}} \cdot \boldsymbol{\lambda} = \omega$ and $\dot{\mathbf{n}} \cdot \dot{\mathbf{n}} \equiv \omega^2$, provide different evolution equations for Φ_p . This is the unexpected consequence of employing precessional equation appropriate for \mathbf{L} to evolve the \mathbf{L}_N -based precessing source frame. It is not difficult to deduce that this essentially arises from the non-vanishing 1.5PN order $\Omega_e^l \times \mathbf{n}$ contributions to $\dot{\mathbf{n}}$ listed in the above equation. The following arguments can also be used to clarify why the above two versions of the same adiabatic condition for the circular orbits result in two different expressions for Φ_p . In our opinion, this arises by identifying $\mathbf{k} \times \mathbf{n}$ to be $\boldsymbol{\lambda} = \mathbf{l} \times \mathbf{n}$, where \mathbf{k} is the unit vector along \mathbf{L} . Strictly speaking, the precessing source frame of [37] is based on \mathbf{L} rather than \mathbf{L}_N due to the use of Ω_k that provides the precessional equation for \mathbf{L} [44, 45]. This implies that their co-moving triad is rather \mathbf{L} -based and the expression for $\dot{\mathbf{n}}$ got components along $\mathbf{k} \times \mathbf{n}$ instead of $\boldsymbol{\lambda} = \mathbf{l} \times \mathbf{n}$. Therefore, $\dot{\mathbf{n}} \cdot \boldsymbol{\lambda}$ results in PN corrections to Φ_p as $(\mathbf{k} \times \mathbf{n}) \cdot \boldsymbol{\lambda}$ is unity only at the leading order (this may be deduced from our equation (8) listed below). This leads to a differential equation for Φ_p that involves PN corrections to ω .

The use of precessional equation appropriate for \mathbf{L} while implementing the precessing convention of [37] motivated us to develop a \mathbf{k} -based precessing convention for constructing inspiral waveforms for spinning compact binaries. This should also allow to explore the practical implications of using the adiabatic approximation to evolve \mathbf{L}_N in the usual implementation of the precessing convention.

2.2. Inspiral waveforms via an \mathbf{L} -based precessing convention

Influenced by the above arguments and [37], we first introduce a \mathbf{k} -based precessing source frame: $(\mathbf{e}_1, \mathbf{e}_2, \mathbf{e}_3 \equiv \mathbf{k})$. The precessional dynamics of $\mathbf{e}_1, \mathbf{e}_2$ and \mathbf{e}_3 are provided by $\dot{\mathbf{e}}_{1,2,3} = \Omega_e \times \mathbf{e}_{1,2,3}$, where $\Omega_e \equiv \Omega_k - (\Omega_k \cdot \mathbf{k}) \mathbf{k}$ and Ω_k is the precessional frequency of \mathbf{k} . It should be obvious that $\dot{\mathbf{e}}_3 = \Omega_e \times \mathbf{e}_3$ is identical to $\dot{\mathbf{e}}_3 = \Omega_k \times \mathbf{e}_3$ as $\mathbf{e}_3 \equiv \mathbf{k}$. It is possible to construct a \mathbf{k} -based co-moving triad $(\mathbf{n}, \boldsymbol{\xi} = \mathbf{k} \times \mathbf{n}, \mathbf{k})$ and introduce an orbital phase Φ such that

$$\mathbf{n} = \cos \Phi \mathbf{e}_1 + \sin \Phi \mathbf{e}_2, \quad (3a)$$

$$\boldsymbol{\xi} = -\sin \Phi \mathbf{e}_1 + \cos \Phi \mathbf{e}_2. \quad (3b)$$

It is fairly straightforward to obtain following expressions for the time derivatives of \mathbf{n} and $\boldsymbol{\xi}$

$$\dot{\mathbf{n}} = \dot{\Phi} \boldsymbol{\xi} + \Omega_e \times \mathbf{n}, \quad (4a)$$

$$\dot{\boldsymbol{\xi}} = -\dot{\Phi} \mathbf{n} + \Omega_e \times \boldsymbol{\xi}. \quad (4b)$$

We are now in a position to obtain the differential equation for Φ . This is derived with the help of the frame independent adiabatic condition for circular orbits, namely $\dot{\mathbf{n}} \cdot \dot{\mathbf{n}} \equiv \omega^2$. Employing the above expression for $\dot{\mathbf{n}}$ in such an adiabatic condition leads to

$$\omega^2 = \dot{\Phi}^2 + \Omega_{e\xi}^2, \quad (5)$$

where $\Omega_{e\xi} = \Omega_e \cdot \boldsymbol{\xi}$ is given by

$$\Omega_{e\xi} = \frac{c^3}{Gm} x^3 \left\{ \delta_1 q \chi_1 (\mathbf{s}_1 \cdot \boldsymbol{\xi}) + \frac{\delta_2}{q} \chi_2 (\mathbf{s}_2 \cdot \boldsymbol{\xi}) \right\}. \quad (6)$$

This results in the following 3PN accurate differential equation for $\dot{\Phi}$

$$\dot{\Phi} = \frac{c^3}{Gm} x^{3/2} \left\{ 1 - \frac{x^3}{2} \left[\delta_1 q \chi_1(\mathbf{s}_1 \cdot \boldsymbol{\xi}) + \frac{\delta_2}{q} \chi_2(\mathbf{s}_2 \cdot \boldsymbol{\xi}) \right]^2 \right\}. \quad (7)$$

These additional terms appear at the 3PN order as we employ equation (1) for $\boldsymbol{\Omega}_k$ that only incorporates the leading order spin-orbit interactions appearing at 1.5PN order. It is not difficult to deduce that the inclusion of 2PN order spin-spin interaction terms in $\boldsymbol{\Omega}_k$ can lead to certain 4PN order contributions to the $\dot{\Phi}$ equation. Additionally, the presence of the above 3PN contributions to $\dot{\Phi}$ equation may be attributed to the fact that the orbital velocity \mathbf{v} can have non-vanishing PN order components along \mathbf{L} while considering generic spinning compact binaries [44].

The use of \mathbf{L} to describe binary orbits also modifies the evolution equation for ω (or x). This is because the spin-orbit interactions are usually incorporated in terms of $\mathbf{s}_1 \cdot \mathbf{l}$ and $\mathbf{s}_2 \cdot \mathbf{l}$, in the literature [21, 37]. These terms require modifications due to the following 1.5PN order relation connecting \mathbf{l} and \mathbf{k}

$$\begin{aligned} \mathbf{l} = \mathbf{k} + x^{3/2} \left\{ -\frac{1}{2} \eta \left[\chi_1(\mathbf{s}_1 \cdot \mathbf{n}) + \chi_2(\mathbf{s}_2 \cdot \mathbf{n}) \right] \mathbf{n} \right. \\ + \left[2 X_1^2 \chi_1(\mathbf{s}_1 \cdot \boldsymbol{\xi}) + \eta \chi_1(\mathbf{s}_1 \cdot \boldsymbol{\xi}) \right. \\ \left. \left. + 2 X_2^2 \chi_2(\mathbf{s}_2 \cdot \boldsymbol{\xi}) + \eta \chi_2(\mathbf{s}_2 \cdot \boldsymbol{\xi}) \right] \boldsymbol{\xi} \right\}, \end{aligned} \quad (8)$$

where $X_1 = m_1/m$ and $X_2 = m_2/m$. The above relation can easily be extracted, for example, from equations (6.10) and (7.10) in [24]. This relation leads to certain additional 3PN order contributions to \dot{x} while describing the binary orbits with \mathbf{k} . These additional terms are, for example, with respect to equation (3.16) of [28] that provides PN accurate expression for dx/dt while invoking \mathbf{l} to describe binary orbits. Our additional contributions to \dot{x} appear at 3PN order as the dominant spin-orbit interactions, in terms of $\mathbf{s}_1 \cdot \mathbf{l}$ and $\mathbf{s}_2 \cdot \mathbf{l}$, contribute to the x evolution equation at 1.5PN order. The differential equation for x in our approach may be written as

$$\begin{aligned} \frac{dx}{dt} = \frac{dx}{dt} (\text{Equation (3.16) in [28]; } \mathbf{l} \rightarrow \mathbf{k}) \\ + \frac{64}{5} \frac{c^3}{Gm} \eta x^5 \left\{ x^3 \left[-\frac{47}{3} X_1^2 \chi_1 \left[-\frac{1}{2} \eta \left(\chi_1(\mathbf{s}_1 \cdot \mathbf{n}) + \chi_2(\mathbf{s}_2 \cdot \mathbf{n}) \right) (\mathbf{s}_1 \cdot \mathbf{n}) \right. \right. \right. \\ + \left. \left. \left(2 X_1^2 \chi_1(\mathbf{s}_1 \cdot \boldsymbol{\xi}) + \eta \chi_1(\mathbf{s}_1 \cdot \boldsymbol{\xi}) + 2 X_2^2 \chi_2(\mathbf{s}_2 \cdot \boldsymbol{\xi}) + \eta \chi_2(\mathbf{s}_2 \cdot \boldsymbol{\xi}) \right) (\mathbf{s}_1 \cdot \boldsymbol{\xi}) \right] \right. \\ - \frac{47}{3} X_2^2 \chi_2 \left[-\frac{1}{2} \eta \left(\chi_1(\mathbf{s}_1 \cdot \mathbf{n}) + \chi_2(\mathbf{s}_2 \cdot \mathbf{n}) \right) (\mathbf{s}_2 \cdot \mathbf{n}) \right. \\ + \left. \left. \left(2 X_1^2 \chi_1(\mathbf{s}_1 \cdot \boldsymbol{\xi}) + \eta \chi_1(\mathbf{s}_1 \cdot \boldsymbol{\xi}) + 2 X_2^2 \chi_2(\mathbf{s}_2 \cdot \boldsymbol{\xi}) + \eta \chi_2(\mathbf{s}_2 \cdot \boldsymbol{\xi}) \right) (\mathbf{s}_2 \cdot \boldsymbol{\xi}) \right] \right. \\ - \frac{25}{4} (X_1 - X_2) X_2 \chi_2 \left[-\frac{1}{2} \eta \left(\chi_1(\mathbf{s}_1 \cdot \mathbf{n}) + \chi_2(\mathbf{s}_2 \cdot \mathbf{n}) \right) (\mathbf{s}_2 \cdot \mathbf{n}) \right. \\ + \left. \left. \left(2 X_1^2 \chi_1(\mathbf{s}_1 \cdot \boldsymbol{\xi}) + \eta \chi_1(\mathbf{s}_1 \cdot \boldsymbol{\xi}) + 2 X_2^2 \chi_2(\mathbf{s}_2 \cdot \boldsymbol{\xi}) + \eta \chi_2(\mathbf{s}_2 \cdot \boldsymbol{\xi}) \right) (\mathbf{s}_2 \cdot \boldsymbol{\xi}) \right] \right. \\ + \frac{25}{4} (X_1 - X_2) X_1 \chi_1 \left[-\frac{1}{2} \eta \left(\chi_1(\mathbf{s}_1 \cdot \mathbf{n}) + \chi_2(\mathbf{s}_2 \cdot \mathbf{n}) \right) (\mathbf{s}_1 \cdot \mathbf{n}) \right. \\ \left. \left. + \left(2 X_1^2 \chi_1(\mathbf{s}_1 \cdot \boldsymbol{\xi}) + \eta \chi_1(\mathbf{s}_1 \cdot \boldsymbol{\xi}) + 2 X_2^2 \chi_2(\mathbf{s}_2 \cdot \boldsymbol{\xi}) + \eta \chi_2(\mathbf{s}_2 \cdot \boldsymbol{\xi}) \right) (\mathbf{s}_1 \cdot \boldsymbol{\xi}) \right] \right\}, \end{aligned} \quad (9)$$

where the first term is adapted from equation (3.16) in [28] by replacing its \mathbf{l} vectors by our \mathbf{k} vectors. Clearly, these additional *spin*-squared terms contribute to dx/dt at 3PN order. Note that the use of \mathbf{k} for \mathbf{l} in the leading order spin-spin contributions to dx/dt , as listed in equation (1) of [37], results in additional 3.5PN order *spin*-cubed terms. Such contributions to our dx/dt equation are neglected as the LALSUITE SpinTaylorT4 code that implement the \mathbf{L}_N -based precessing convention does not include any *spin*-cubed terms in its differential equation for x .

In what follows, we model inspiral GWs from spinning compact binaries in our \mathbf{k} -based precessing convention. We begin by displaying the following quadrupolar order expressions for the two GW polarization states:

$$h_{\times}|_Q(t) = 2 \frac{G m \eta x}{c^2 R'} (2 \xi_x \xi_y - 2 n_x n_y), \quad (10a)$$

$$h_{+}|_Q(t) = 2 \frac{G m \eta x}{c^2 R'} (\xi_x^2 - \xi_y^2 - n_x^2 + n_y^2), \quad (10b)$$

where $\xi_{x,y}$ and $n_{x,y}$ are the x and y components of $\boldsymbol{\xi}$ and \mathbf{n} in an inertial frame associated with \mathbf{N} , the unit vector that points from the source to the detector, while R' is the distance to the binary. These x and y components can be expressed in terms of the Cartesian components of \mathbf{e}_1 and \mathbf{e}_2 via equations (3). We note that the above expressions for the quadrupolar order h_{\times} and h_{+} are written in the so-called frame-less convention [21]. These expressions emerge from the following standard definitions for the quadrupolar order GW polarization states:

$$h_{\times}|_Q(t) = \frac{1}{2} (p^i q^j + q^i p^j) h_{ij}^{\text{TT}}|_Q, \quad (11a)$$

$$h_{+}|_Q(t) = \frac{1}{2} (p^i p^j - q^i q^j) h_{ij}^{\text{TT}}|_Q, \quad (11b)$$

where \mathbf{p} and \mathbf{q} are the two polarization vectors forming, along with \mathbf{N} , an orthonormal right-handed triad. To obtain equation (10), we used the following expression for the quadrupolar order transverse-traceless part of the far-zone field $h_{ij}^{\text{TT}}|_Q$

$$h_{ij}^{\text{TT}}|_Q = \frac{4 G m \eta x}{c^2 R'} (\xi^i \xi^j - n^i n^j). \quad (12)$$

In the frame-less convention, we let the components of \mathbf{p} and \mathbf{q} in the \mathbf{N} -based inertial frame to be $\mathbf{p} = (1, 0, 0)$ and $\mathbf{q} = (0, 1, 0)$. Clearly, we need to specify how the Cartesian components of $\boldsymbol{\xi}$ and \mathbf{n} vary in time to obtain temporally evolving GW polarization states for inspiralling generic spinning compact binaries. Therefore, we require to solve numerically the differential equations for Φ, x, \mathbf{e}_1 and \mathbf{e}_2 to obtain $h_{\times}|_Q(t)$ and $h_{+}|_Q(t)$. We use equation (7) for Φ while the differential equation for x is given by equation (9) that contains all the non-spinning contributions accurate up to 3.5PN order and the usual spin contributions that are fully 2PN accurate. These contributions are provided, for example, by equation (3.16) in [28] and are listed in the Appendix A, where we have replaced \mathbf{l} by \mathbf{k} . These specific PN order choices are influenced by the fact that the LALSUITE SpinTaylorT4 code also employs an evolution equation for ω that incorporates such PN contributions. We note that this routine implements the \mathbf{l} -based precessing convention of [37] to construct inspiral templates to search for GWs from generic spinning binaries. The differential equations for \mathbf{e}_1 and \mathbf{e}_2 in our approach are given by

$$\dot{\mathbf{e}}_1 = \boldsymbol{\Omega}_e \times \mathbf{e}_1 = (\boldsymbol{\Omega}_k - (\boldsymbol{\Omega}_k \cdot \mathbf{k})) \times \mathbf{e}_1, \quad (13a)$$

$$\dot{\mathbf{e}}_2 = \boldsymbol{\Omega}_e \times \mathbf{e}_2 = (\boldsymbol{\Omega}_k - (\boldsymbol{\Omega}_k \cdot \mathbf{k})) \times \mathbf{e}_2, \quad (13b)$$

where we use the following expression for $\boldsymbol{\Omega}_k$ that incorporates the leading order spin-orbit and spin-spin interactions

$$\boldsymbol{\Omega}_k = \frac{c^3}{Gm} x^3 \left\{ \delta_1 q \chi_1 \mathbf{s}_1 + \frac{\delta_2}{q} \chi_2 \mathbf{s}_2 - \frac{3}{2} x^{1/2} \eta \chi_1 \chi_2 [(\mathbf{k} \cdot \mathbf{s}_1) \mathbf{s}_2 + (\mathbf{k} \cdot \mathbf{s}_2) \mathbf{s}_1] \right\}. \quad (14)$$

It is fairly straightforward to verify that this expression is identical to the coefficient of $\dot{\mathbf{L}}_N$ appearing on the right hand side of equation (9) in [37]. The above equations imply that we also need to invoke the precessional equations for \mathbf{s}_1 , \mathbf{s}_2 and \mathbf{k} (or \mathbf{e}_3) to tackle numerically the dynamics of such binaries. The three coupled equations for \mathbf{s}_1 , \mathbf{s}_2 and \mathbf{k} that include the leading order spin-orbit and spin-spin interactions read

$$\dot{\mathbf{s}}_1 = \frac{c^3}{Gm} x^{5/2} \left\{ \delta_1 (\mathbf{k} \times \mathbf{s}_1) + \frac{1}{2} x^{1/2} \left[X_2^2 \chi_2 (\mathbf{s}_2 \times \mathbf{s}_1) - 3 X_2^2 \chi_2 (\mathbf{k} \cdot \mathbf{s}_2) (\mathbf{k} \times \mathbf{s}_1) \right] \right\}, \quad (15a)$$

$$\dot{\mathbf{s}}_2 = \frac{c^3}{Gm} x^{5/2} \left\{ \delta_2 (\mathbf{k} \times \mathbf{s}_2) + \frac{1}{2} x^{1/2} \left[X_1^2 \chi_1 (\mathbf{s}_1 \times \mathbf{s}_2) - 3 X_1^2 \chi_1 (\mathbf{k} \cdot \mathbf{s}_1) (\mathbf{k} \times \mathbf{s}_2) \right] \right\}, \quad (15b)$$

$$\begin{aligned} \dot{\mathbf{k}} = \frac{c^3}{Gm} x^3 \left\{ \delta_1 q \chi_1 (\mathbf{s}_1 \times \mathbf{k}) + \frac{\delta_2}{q} \chi_2 (\mathbf{s}_2 \times \mathbf{k}) \right. \\ \left. - \frac{3}{2} x^{1/2} \eta \chi_1 \chi_2 [(\mathbf{k} \cdot \mathbf{s}_1) (\mathbf{s}_2 \times \mathbf{k}) + (\mathbf{k} \cdot \mathbf{s}_2) (\mathbf{s}_1 \times \mathbf{k})] \right\}. \end{aligned} \quad (15c)$$

It is not very difficult to verify that the above equations for $\dot{\mathbf{s}}_1$ and $\dot{\mathbf{s}}_2$ are identical to equations (2) and (3) in [37] while the differential equation for \mathbf{k} , as expected, arises from the usual conservation of total angular momentum \mathbf{J} . This conservation implies that $L \dot{\mathbf{k}} = -S_1 \dot{\mathbf{s}}_1 - S_2 \dot{\mathbf{s}}_2$. We would like to state again that the equations (7), (A.1), (A.2) and (9) provide the differential equations for Φ and x in the present implementation of \mathbf{k} -based precessing convention. Strictly speaking, the use of equation (14) for $\boldsymbol{\Omega}_k$ requires us to include the additional 4PN and 3.5PN contribution to $d\Phi/dt$ and dx/dt , respectively. However, we do not incorporate such spin-quartic and spin-cubic terms in our present work.

In practice, we numerically solve simultaneously the differential equations for \mathbf{e}_1 , \mathbf{k} , \mathbf{s}_1 , \mathbf{s}_2 , Φ and x to obtain temporally evolving Cartesian components of \mathbf{n} and $\boldsymbol{\xi}$. The resulting variations in these Cartesian components are imposed on the expressions for $h_{\times,+}|_Q(t)$, given by equations (10). This leads to inspiral waveforms for generic spinning compact binaries in our \mathbf{k} -based precessing convention. Note that we do not solve the differential equation for \mathbf{e}_2 . This is because the temporal evolution of \mathbf{e}_2 can be estimated using the relation $\mathbf{e}_2(t) = \mathbf{k}(t) \times \mathbf{e}_1(t)$. This implies that we solve 12 differential equations for the Cartesian components of \mathbf{e}_1 , \mathbf{k} , \mathbf{s}_1 and \mathbf{s}_2 along with the differential equations for Φ and x to track the time evolution for the Cartesian components of \mathbf{n} and $\boldsymbol{\xi}$. The required initial values for the Cartesian components of \mathbf{e}_1 , \mathbf{k} , \mathbf{s}_1 and \mathbf{s}_2 are given by freely choosing the following five angles: θ_{10} , ϕ_{10} , θ_{20} , ϕ_{20} and ι_0 . These angles specify the above four unit vectors in the \mathbf{N} -based inertial

frame at the initial epoch such that

$$\mathbf{s}_1 = (\sin \theta_{10} \cos \phi_{10}, \sin \theta_{10} \sin \phi_{10}, \cos \theta_{10}) , \quad (16a)$$

$$\mathbf{s}_2 = (\sin \theta_{20} \cos \phi_{20}, \sin \theta_{20} \sin \phi_{20}, \cos \theta_{20}) , \quad (16b)$$

$$\mathbf{k} = (\sin \iota_0, 0, \cos \iota_0) , \quad (16c)$$

$$\mathbf{e}_1 = (\cos \iota_0, 0, -\sin \iota_0) . \quad (16d)$$

This choice is also influenced by the LALSUITE SpinTaylorT4 code of LSC. Additionally, we let the initial x value to be $x_0 = (G m \omega_0 / c^3)^{2/3}$ where $\omega_0 = 10\pi$ Hz and the initial phase Φ_0 to be zero.

We move on to explain how to specify initial conditions, physically identical to equations (16), while constructing inspiral waveforms based on the \mathbf{l} -based precessing convention. Clearly, the initial orientations of two spin vectors in the inertial \mathbf{N} frame should be identical in the two approaches. However, the orientation of \mathbf{l} in such an inertial frame is different from that of \mathbf{k} . We compute $\mathbf{N} \cdot \mathbf{l}$ using equation (8) that provide 1.5PN accurate relation connecting \mathbf{l} and \mathbf{k} . This PN relation makes the value of $\mathbf{N} \cdot \mathbf{l}$ at x_0 to depend on $\iota_0, m, \eta, \chi_1, \chi_2, \Phi_0$ and the four angles that specify \mathbf{s}_1 and \mathbf{s}_2 in the inertial \mathbf{N} frame. We observe that $[\mathbf{N} \cdot \mathbf{l}(x_0) - \mathbf{N} \cdot \mathbf{k}(x_0)]$ is maximum for equal mass maximally spinning compact binaries and the difference is usually less than 0.1%. The value of $\mathbf{N} \cdot \mathbf{l}(x_0)$ specifies the initial orientation of \mathbf{l} in the inertial \mathbf{N} frame as we usually let its azimuthal angle to be zero along with $\Phi_p(x_0)$ (we have verified that the changes in these angles play no role in our match computations). The difference in $\mathbf{N} \cdot \mathbf{l}(x_0)$ and $\mathbf{N} \cdot \mathbf{k}(x_0)$ values leads to slightly different values for $\mathbf{k} \cdot \mathbf{s}_1$ and $\mathbf{l} \cdot \mathbf{s}_1$ at the initial epoch. Therefore, the orbital frequency and phase evolutions are slightly different in the two approaches even in the absence of our 3PN order additional terms. We observe that the differences in these two dot products, namely $\mathbf{k} \cdot \mathbf{s}_1$ and $\mathbf{l} \cdot \mathbf{s}_1$, have their maximum values for equal mass maximally spinning compact binaries. In the next section, we pursue the *match* computations to probe the implications of additional 3PN order terms present in the frequency and phase evolution equations while constructing our \mathbf{k} -based inspiral waveforms.

3. Match computations involving the above two families of inspiral waveforms

We employ the *match*, detailed in [11, 42], to compare inspiral waveforms constructed via the above described \mathbf{l} and \mathbf{k} -based precessing conventions. Our comparison is influenced (and justified) by the fact that the precessing source frames of the above two conventions are functionally identical. This should be evident from the use of *the same* precessional frequency, appropriate for \mathbf{k} , to obtain PN accurate expressions for both the \mathbf{l} -based Ω_e^l and \mathbf{k} -based Ω_e . Therefore, the *match* estimates probe influences of the additional 3PN order terms present in the differential equations for Φ and x in our approach. Additionally, we have verified that these 3PN order terms are not present in the usual implementation of the precessing convention as provided by the LALSUITE SpinTaylorT4 code.

Our match $\mathcal{M}(h_l, h_k)$ computations involve h_l and h_k , the two families of inspiral waveforms arising from the \mathbf{l} and \mathbf{k} -based precessing conventions. The h_l inspiral waveform families are adapted from the LALSUITE SpinTaylorT4 code of LSC while h_k families, as expected, arise from our approach (equations (10)). It should be noted that we employ the quadrupolar (Newtonian) order expressions for $h_{\times,+}$ while computing h_l

and h_k in the present analysis. However, the LALSUITE SpinTaylorT4 code can provide waveforms that include 1.5PN order corrections to their amplitudes. We would like to stress that the two families involved in our $\mathcal{M}(h_l, h_k)$ computations are characterized by identical values of m, η, χ_1 and χ_2 . Additionally, the initial orientations of the two spins in the \mathbf{N} -based inertial frame were also chosen to be identical. The computation of $\mathbf{N} \cdot \mathbf{l}$ from $\mathbf{N} \cdot \mathbf{k}$ with the help of equation (8) ensures that \mathbf{l} and \mathbf{k} orientations at the initial epoch are physically equivalent. Therefore, our $\mathcal{M}(h_l, h_k)$ computations indeed compare two waveform families with physically equivalent orbital and spin configurations at the initial epoch. To obtain a specific $\mathcal{M}(h_l, h_k)$ estimate, we first compute an overlap function between the relevant h_l and h_k inspiral waveforms:

$$\mathcal{O}(h_l, h_k) = \langle \hat{h}_l, \hat{h}_k \rangle = \frac{\langle h_l | h_k \rangle}{\sqrt{\langle h_l | h_l \rangle \langle h_k | h_k \rangle}}, \quad (17)$$

where \hat{h}_l and \hat{h}_k stand for the normalized $h_l(t)$ and $h_k(t)$ waveforms, respectively. The angular bracket between h_l and h_k defines certain noise weighted inner product, namely

$$\langle h_l | h_k \rangle = 4 \operatorname{Re} \int_{f_{\text{low}}}^{f_{\text{cut}}} \frac{\tilde{h}_l^*(f) \tilde{h}_k(f)}{S_h(f)} df. \quad (18)$$

In the above equation, $\tilde{h}_l(f)$ and $\tilde{h}_k(f)$ stand for the Fourier transforms of $h_l(t)$ and $h_k(t)$, while $S_h(f)$ denotes the one-sided power spectral density. We have invoked the zero-detuned, high power sensitivity curve of aLIGO [46] in our $\mathcal{M}(h_l, h_k)$ computations. The upper cut-off frequency f_{cut} is chosen to be $c^3/(G m \pi 10^{3/2})$ while the lower cut-off frequency f_{low} , associated with the GW detector, equals 10 Hz. The match $\mathcal{M}(h_l, h_k)$ is computed by maximizing the $\mathcal{O}(h_l, h_k)$ over two extrinsic variables, namely the time of arrival t_0 and the overall phase ϕ_0 of GW at time t_0 [47]. This leads to

$$\mathcal{M} = \max_{t_0, \phi_0} \mathcal{O}(h_l, h_k). \quad (19)$$

The maximizations of over t_0 and ϕ_0 are performed by following [11]. We perform the maximization over t_0 via the FFT algorithm while the maximization over ϕ_0 requires us to deploy two orthogonal templates. Let us emphasize that we terminate h_l and h_k inspiral waveform families when their respective x parameters reach 0.1 which roughly corresponds to orbital separations $\sim 10 G m / c^2$. This choice arguably ensures the validity of PN approximation to describe the temporal evolutions of the above two families in our $[f_{\text{low}}-f_{\text{cut}}]$ frequency window. Therefore, it is reasonable to associate the departure of \mathcal{M} estimates from unity to the additional 3PN order contributions to the differential equations for the orbital phase and the associated angular frequency.

We move on to list results of some of our \mathcal{M} computations. It is not very difficult to realize that extensive \mathcal{M} computations that deal with all aLIGO relevant spin and binary configurations will be rather difficult to achieve. Therefore, we restrict our attention to a selected number of binaries to compare the $h_l(t)$ and $h_k(t)$ inspiral waveform families. In our match computations, we mainly consider binaries having total mass $m \geq 30 M_\odot$ due to the following two reasons. First, it is comparatively expensive (computationally) to generate lengthy inspiral waveforms for low mass binaries in the aLIGO frequency window. Additionally, we are interested in to explore the dependence of our \mathcal{M} estimates on the mass ratio q in the $[1 - 10]$ range. Clearly, low m binaries can lead to secondary BHs having masses lower than

the usual neutron star masses for high q cases. In figure 1, we consider maximally spinning BH binaries, characterized by the total mass $m = 30M_\odot$, while varying the mass ratio q from unity to 10. The left and right panel plots are for configurations having initial dominant spin-orbit misalignments $\tilde{\theta}_1(x_0)$ ($\cos^{-1}(\mathbf{k} \cdot \mathbf{s}_1)$) given by 30° and 60° , respectively. Additionally, we let the initial orbital plane orientation in the \mathbf{N} -based inertial frame to take two values leading to edge-on ($\iota_0 = 90^\circ$) and face-on ($\iota_0 = 0^\circ$) binary orientations. These binary configurations, characterized by two different spin-orbit misalignments and orbital plane orientations in the \mathbf{N} -based inertial frame, are obtained by choosing appropriately different values for the more massive BH initial spin orientation, namely $\theta_1(x_0)$ in equation (16a). For example, we choose θ_{10} to be 30° and 60° to get $\tilde{\theta}_1(x_0)$ equals 30° and 60° , respectively, for face-on binaries. However, in the case of edge-on binaries, we require to choose θ_{10} to be 60° and 30° , respectively. All other initial angular variables, appearing in equations (16a) and (16b), were chosen to be $\phi_{10} = 0^\circ$, $\theta_{20} = 20^\circ$, $\phi_{20} = 90^\circ$ (we have verified that the \mathcal{M} estimates are rather insensitive to the choice of these initial angular variables). Let us note that \mathbf{l} orientations (from \mathbf{N}) for these configurations will be slightly different from 0° or 90° due to the 1.5PN accurate relation between \mathbf{l} and \mathbf{k} .

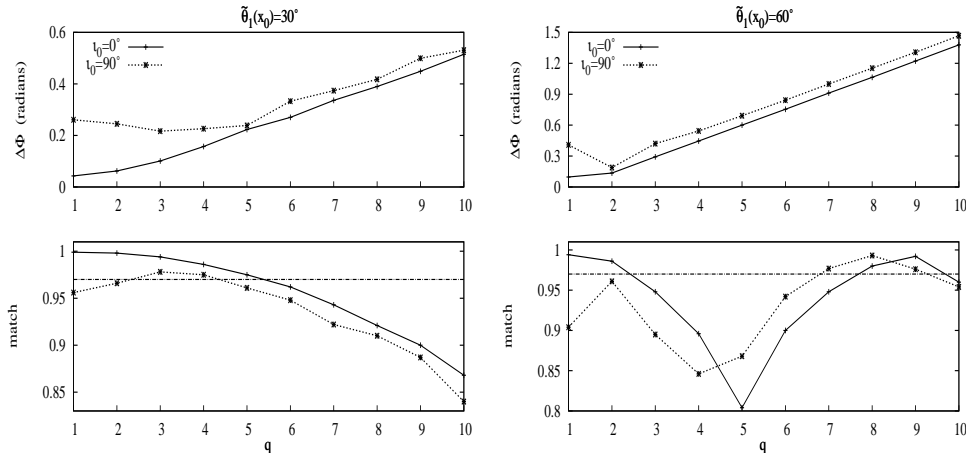


Figure 1. Plots for the accumulated orbital phase ($\Delta\Phi$) and the associated match (\mathcal{M}) estimates as functions of the mass ratio q for maximally spinning $m = 30M_\odot$ BH binaries inspiralling in the $[f_{\text{low}}-f_{\text{cut}}]$ frequency interval. The left and right panel plots are for binaries having dominant spin-orbit misalignments $\tilde{\theta}_1 = 30^\circ$ and 60° , respectively, at x_0 . The solid line plots in each panel correspond to face-on binaries whereas the dotted line curves are for edge-on binaries. We find a gradual degradation of the \mathcal{M} estimates for higher q values for $\tilde{\theta}_1 = 30^\circ$ binaries. However, this trend is not visible for $\tilde{\theta}_1 = 60^\circ$ binaries. These configurations with different spin-orbit misalignments and binary orientations are obtained by setting different values for θ_{10} and ι_0 . Face-on binaries with $\tilde{\theta}_1(x_0) = 30^\circ$ and 60° have (θ_{10}, ι_0) as $(30^\circ, 0^\circ)$ and $(60^\circ, 0^\circ)$ while the edge-on binaries have (θ_{10}, ι_0) as $(60^\circ, 90^\circ)$ and $(30^\circ, 90^\circ)$, respectively. The initial values of the other angular parameters remain the same, namely $\phi_{10} = 0^\circ$, $\theta_{20} = 20^\circ$, $\phi_{20} = 90^\circ$. The PN accurate relation between \mathbf{k} and \mathbf{l} also results in slightly different dominant spin-orbit misalignments in the two approaches.

The upper and lower row plots in figure 1 are for $\Delta\Phi$, the accumulated orbital phase differences in the $[f_{\text{low}}-f_{\text{cut}}]$ frequency interval while dealing with the h_l and

h_k inspiral waveforms and the associated $\mathcal{M}(h_l, h_k)$ estimates, respectively. We find that the variations in \mathcal{M} estimates are quite independent of the initial orbital plane orientations. However, variation in match estimates do depend on the initial dominant spin-orbit misalignment and the mass ratio q . The left panel plots show gradual decrease in \mathcal{M} values as we increase the q value and this variation is reflected in the gradual increase of $\Delta\Phi$. Incidentally, this pattern is also observed for configurations having somewhat smaller initial dominant spin-orbit misalignments. However, the \mathcal{M} estimates are close to unity for tiny $\tilde{\theta}_1(x_0)$ values and this is expected as precessional effects are minimal for such binaries. Therefore, the effect of the above discussed additional 3PN order terms are more pronounced for high q compact binaries having *moderate* dominant spin-orbit misalignments. This picture is modified for binaries having substantial dominant spin-orbit misalignments as evident from the \mathcal{M} plots in the right panel of figure 1. For such binaries, the \mathcal{M} estimates dip to a minimum and recover as we vary q from 1 to 10 for both edge-on and face-on orbital plane orientations. In contrast, we observe a gradual increase in $\Delta\Phi(q)$. The monotonic increment in $\Delta\Phi(q)$ plots is essentially due to the presence of $X_1 - X_2$ terms in the additional 3PN order contributions to dx/dt , given by equation (9). This is because $X_1 - X_2$ terms are absent for equal mass binaries which leads to smaller $\Delta\Phi$ estimates for smaller q value binaries. However, it is not possible to explain the observed $\mathcal{M}(q)$ variations purely in terms the displayed $\Delta\Phi(q)$ values, especially when precessional effects are substantial as in the $\tilde{\theta}_1(x_0) = 60^\circ$ cases. We observe that the initial values of angles like $\cos^{-1}(\mathbf{k} \cdot \mathbf{j})$ and $\cos^{-1}(\mathbf{N} \cdot \mathbf{j})$ also influence the precessional modulations in the waveforms, where \mathbf{j} is the unit vector along \mathbf{J} . Therefore, we examined how the initial values of these angles vary as functions of q . We find monotonic increase (decrease) in the initial values of $\cos^{-1}(\mathbf{k} \cdot \mathbf{j})$ ($\cos^{-1}(\mathbf{N} \cdot \mathbf{j})$) when q value is varied from 1 to 10. Therefore, we speculate that the combined effect of such variations and the non-negligible $\Delta\Phi(q)$ values may provide a possible explanation for the dip in match estimates around $q=5$. This is because initial values of the above mentioned angles do define the way various dot products, involving \mathbf{n} , $\boldsymbol{\xi}$, \mathbf{s}_1 and \mathbf{s}_2 , vary in time. It should be noted that these dot products are present in the additional 3PN order terms in the dx/dt expression given by equation (9).

This plausible explanation is tested in figure 2, where we plot $\Delta\Phi(q)$ and $\mathcal{M}(q)$ estimates for binary configurations having three different m values. It is not difficult to infer that the above listed arguments should also hold for such compact binaries. The initial dominant spin-orbit misalignment is again chosen to be 60° while considering only edge-on configurations. All other spin and orbital orientations at the initial epoch are identical to the cases displayed in the right panel plots of figure 1. Clearly, the plots in figure 2 are qualitatively similar to those in the right panel plots of figure 1. However, the dip in \mathcal{M} estimates shifts to higher q values for higher m compact binaries. We conclude from the above two figures that GW data analysis relevant differences between the above two inspiral families are more pronounced for unequal mass BH binaries. Incidentally, we also find similar behavior while plotting $\mathcal{M}(q)$ and $\Phi(q)$ for maximally spinning $m = 20 M_\odot$ BH binaries. In this case, the minimum \mathcal{M} value occurs around $q = 3$ and this is consistent with the trend observed in figure 2. It is reasonable to suspect that the spin-squared additional terms are influential only for maximally spinning BH binaries. However, we observe qualitatively similar $\mathcal{M}(q)$ estimates for binary configurations having moderately spinning BHs ($\chi_1 = \chi_2 = 0.75$) as well as having mildly spinning BHs ($\chi_1 = \chi_2 = 0.5$). Moreover, the $\mathcal{M}(q)$ computations indicate that the effect of additional 3PN order terms in $d\Phi/dt$ and

dx/dt equations are non-negligible even for single-spin compact binaries. In figure 3, we plot $\Delta\Phi(q)$ and $\mathcal{M}(q)$ while considering \mathbf{l} and \mathbf{k} -based single-spin waveforms for $m = 30M_\odot, \theta_1(x_0) = 60^\circ$ binaries in edge-on orientations. We find that these plots fairly resemble their double spin counterparts shown in the right panel plots of figure 1. Additionally, the variations in the initial values of $\cos^{-1}(\mathbf{k} \cdot \mathbf{j})$ and $\cos^{-1}(\mathbf{N} \cdot \mathbf{j})$ are similar to the double spin binaries, while varying q value from 1 to 10. Therefore, we conclude that it may be beneficial to keep the additional 3PN order terms in the differential equations for Φ and x while modeling inspiral GWs even from single-spin binaries via the precessing convention.

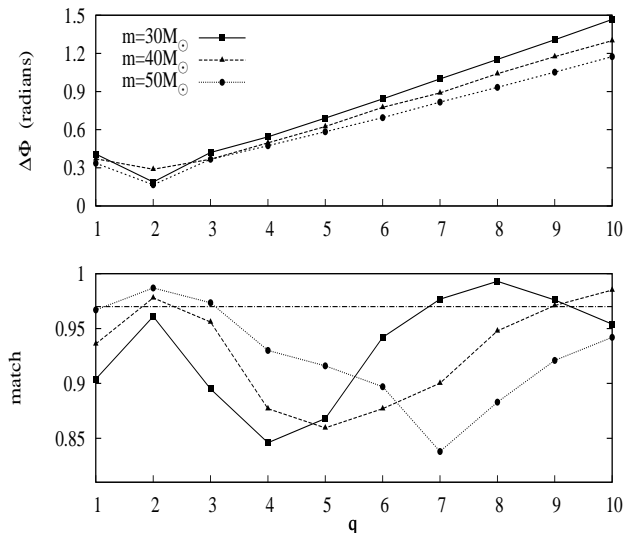


Figure 2. Plots that display variations in $\Delta\Phi$ and \mathcal{M} as functions of q for edge-on maximally spinning BH binaries having $m = 30 M_\odot, 40 M_\odot$ and $50 M_\odot$ while keeping $\theta_1(x_0)$ to be 60° . All other initial angular parameters are identical to those used in the right panel plots of figure 1. The position of the dip in $\mathcal{M}(q)$ plots is shifted towards higher q values for higher m binaries. A possible explanation relies on the more influential contributions from the various dot products that appear in equation (9) for such binaries having q roughly in the 4 to 9 range.

The LSC also developed LALSUITE SpinTaylorT2 code that employs a slightly different version of dx/dt equation while implementing the \mathbf{l} -based precessing convention. Note that it is possible to construct various PN approximants to model inspiral GWs by using the same PN accurate expressions for the conserved energy, far-zone energy flux and the *energy balance argument* [14]. The differential equation for x in the SpinTaylorT2 approximant arises from the following considerations. We begin by displaying (symbolically) the 3.5PN accurate expression for dx/dt , employed in the LALSUITE SpinTaylorT4 code, as

$$\left. \frac{dx}{dt} \right|_{T4} = \frac{64}{5} \frac{c^3}{Gm} \eta x^5 \left\{ 1 + A_1 x + A_{1.5} x^{3/2} + A_2 x^2 + A_{2.5} x^{5/2} + A_3 x^3 + A_{3.5} x^{7/2} \right\}, \quad (20)$$

where the coefficients A_i are functions of $\eta, \pi, \log(6x)$ and γ_E (Euler's constant) when including only the non-spinning contributions. However, the coefficients from $A_{1.5}$ to

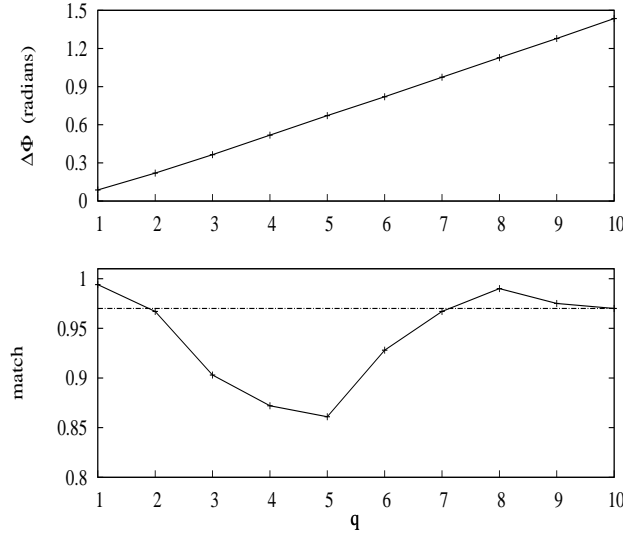


Figure 3. Plots that compare *single-spin* SpinTaylorT4 inspiral waveform families in the \mathbf{l} and \mathbf{k} -based approaches. These $\Delta\Phi(q)$ and $\mathcal{M}(q)$ plots are for edge-on $m = 30M_{\odot}$ binaries containing maximally spinning dominant BH having $\theta_1(x_0) = 60^\circ$. The qualitative and quantitative nature of these plots are essentially identical to the double spin binaries of figure 1.

$A_{3.5}$ additionally depend on $X_1, X_2, (\mathbf{s}_1 \cdot \mathbf{l}), (\mathbf{s}_2 \cdot \mathbf{l}), (\mathbf{s}_1 \cdot \mathbf{s}_2), \chi_1$ and χ_2 to incorporate various spin contributions. The explicit expressions for these A_i coefficients may be obtained either from equation (3.16) in [28] or from the LALSUITE SpinTaylorT4 code itself. With these inputs, one defines the differential equation for x in the SpinTaylorT2 approximant to be

$$\frac{dx}{dt}\Big|_{T2} = \frac{64}{5} \frac{c^3}{Gm} \eta \frac{x^5}{\left\{1 + A_1 x + A_{1.5} x^{3/2} + A_2 x^2 + A_{2.5} x^{5/2} + A_3 x^3 + A_{3.5} x^{7/2}\right\}^{-1}}, \quad (21)$$

$$= \frac{64}{5} \frac{c^3}{Gm} \eta \frac{x^5}{\left\{1 + A'_1 x + A'_{1.5} x^{3/2} + A'_2 x^2 + A'_{2.5} x^{5/2} + A'_3 x^3 + A'_{3.5} x^{7/2}\right\}}. \quad (22)$$

This construction ensures that the coefficients A'_i are going to depend on various A_i coefficients due to the binomial expansion of the denominator of equation (21) that includes all the $x^{7/2}$ contributions. For example, the $A'_{3.5}$ coefficient is going to depend explicitly on all the A_i coefficients whereas the A'_2 coefficient depends only on the A_1 and A_2 coefficients. We observe that the resulting spin-squared terms are usually not incorporated into the A'_3 and $A'_{3.5}$ coefficients in the LALSUITE SpinTaylorT2 code of LSC.

We construct the differential equation for x in our SpinTaylorT2 approximant in a similar manner. Therefore, the various A'_i coefficients are given in terms of A_i coefficients which can be extracted from our equations (9), (A.1) and (A.2) for dx/dt .

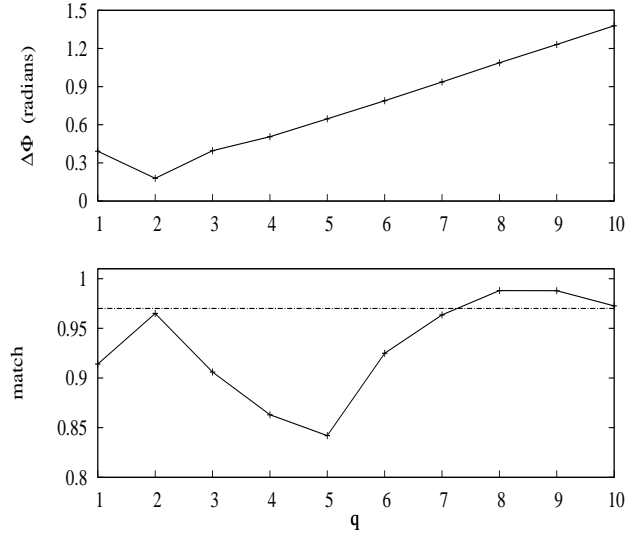


Figure 4. Plots for $\Delta\Phi$ and \mathcal{M} as functions of q that invoke \mathbf{l} and \mathbf{k} -based SpinTaylorT2 approximants. We are dealing with edge-on maximally spinning BH binaries having $m = 30 M_{\odot}$ and $\tilde{\theta}_1(x_0) = 60^\circ$. The $\Delta\Phi$ and \mathcal{M} estimates are similar to those obtained using SpinTaylorT4 approximant as shown in the right panel plots of figure 1.

For example, the expressions for A_2 and A'_2 in our approach are given by

$$\begin{aligned}
A_2 = & \left(\frac{34103}{18144} + \frac{13661}{2016}\eta + \frac{59}{18}\eta^2 \right) - \frac{1}{48}\eta\chi_1\chi_2 \left(247(\mathbf{s}_1 \cdot \mathbf{s}_2) - 721(\mathbf{s}_1 \cdot \mathbf{k})(\mathbf{s}_2 \cdot \mathbf{k}) \right) \\
& + X_1^2 \chi_1^2 \left(\frac{5}{2} (3(\mathbf{s}_1 \cdot \mathbf{k})^2 - 1) + \frac{1}{96} (7 - (\mathbf{s}_1 \cdot \mathbf{k})^2) \right) \\
& + X_2^2 \chi_2^2 \left(\frac{5}{2} (3(\mathbf{s}_2 \cdot \mathbf{k})^2 - 1) + \frac{1}{96} (7 - (\mathbf{s}_2 \cdot \mathbf{k})^2) \right), \tag{23}
\end{aligned}$$

$$\begin{aligned}
A'_2 = & -A_2 + A_1^2, \\
= & - \left[\left(\frac{34103}{18144} + \frac{13661}{2016}\eta + \frac{59}{18}\eta^2 \right) - \frac{1}{48}\eta\chi_1\chi_2 \left(247(\mathbf{s}_1 \cdot \mathbf{s}_2) - 721(\mathbf{s}_1 \cdot \mathbf{k})(\mathbf{s}_2 \cdot \mathbf{k}) \right) \right. \\
& + X_1^2 \chi_1^2 \left(\frac{5}{2} (3(\mathbf{s}_1 \cdot \mathbf{k})^2 - 1) + \frac{1}{96} (7 - (\mathbf{s}_1 \cdot \mathbf{k})^2) \right) \\
& \left. + X_2^2 \chi_2^2 \left(\frac{5}{2} (3(\mathbf{s}_2 \cdot \mathbf{k})^2 - 1) + \frac{1}{96} (7 - (\mathbf{s}_2 \cdot \mathbf{k})^2) \right) \right] + \left[-\frac{743}{336} - \frac{11\eta}{4} \right]^2. \tag{24}
\end{aligned}$$

In the \mathbf{k} -based SpinTaylorT2 approximant, we incorporate our additional 3PN accurate spin-spin terms which contribute *only* to the A'_3 coefficient. In other words, $A'_3 = -A_3 + A_{1.5}^2 + 2A_1A_2 - A_1^3$ contains our additional 3PN order spin-squared terms via the SpinTaylorT4 based A_3 coefficient. We would like to emphasize that we are not incorporating possible 3PN and 3.5PN order spin-spin terms arising due the binomial expansion. This is to make sure that the \mathbf{l} and \mathbf{k} -based SpinTaylorT2 approximants differ only by our additional 3PN order spin-spin terms. We explore the implications of these additional 3PN order terms again with the help of $\mathcal{M}(h_l, h_k)$ computations,

where h_l and h_k now stand for the \mathbf{l} -based and \mathbf{k} -based waveform families that employ the above described PN accurate expressions for dx/dt . In figure 4, we plot $\mathcal{M}(q)$ and $\Delta\Phi(q)$ for edge-on $m = 30 M_\odot$ maximally spinning BH binaries having dominant spin-orbit misalignment equal to 60° at x_0 . The \mathcal{M} and $\Delta\Phi$ estimates are similar to those obtained using SpinTaylorT4 approximant as shown in the right panel plots of figure 1.

It may be argued that the inclusion of our 3PN order spin-squared terms to the differential equation for x is not desirable. This is because we do not incorporate 3PN order contributions to dx/dt that arise from the next-to-leading order spin-spin interactions. These terms are not included as they are yet to be computed in the literature. Clearly, the present match computations should be repeated when these 3PN order contributions are explicitly available. However, this should not prevent one from probing the data analysis implications of the adiabatic approximation employed in the \mathbf{L}_N -based precessing convention of [37]. This could be especially useful while invoking PN accurate differential equation for x that incorporate higher order spin contributions as pursued in LALSUITE SpinTaylorT4 and LALSUITE SpinTaylorT2 codes, developed by the LSC to implement the \mathbf{L}_N -based precessing convention. Hopefully, the data analysis implications of our 3PN order terms should provide additional motivation to explicitly obtain the next-to-leading order spin-spin contributions to dx/dt . In contrast, it should be noted that the additional PN contribution to $d\Phi/dt$, given by equation (7), are fully accurate to 3PN order. The fact that such additional precessional effects enter the expression for $d\Phi/dt$ only at the 3PN order should justify naming our approach as \mathbf{k} -based precessing convention. It is worthwhile to remember that precession induced modulations enter the differential equation for the orbital phase at 1.5PN order in the absence of precessing convention.

4. Conclusions

We developed a precessing convention to model inspiral GWs from generic spinning compact binaries that employs PN accurate orbital angular momentum \mathbf{L} to describe binary orbits and to construct the required precessing source frame. The main motivation for our approach is the usual practice of using PN accurate precessional equation, appropriate for \mathbf{L} , to evolve the Newtonian orbital angular momentum \mathbf{L}_N while constructing inspiral waveforms. We showed that this practice leads to higher order PN corrections to $\dot{\Phi}_p = \omega$ equation. A set of differential equations and the quadrupolar order GW polarization states in certain frame-less convention are developed to model inspiral GWs in our \mathbf{L} -based approach. We explained why the differential equations for the orbital phase and frequency will have additional 3PN order terms in our approach compared to the usual \mathbf{L}_N -based implementation of precessing convention. The influence of these additional 3PN order terms were explored with the help of *match* computations involving \mathbf{L} and \mathbf{L}_N -based inspiral waveforms for spinning compact binaries with physically equivalent orbital and spin configurations at the initial epoch. We adapted both LALSUITE SpinTaylorT4 and LALSUITE SpinTaylorT2 codes, developed by the LSC, while implementing \mathbf{L}_N -based precessing convention. The resulting match estimates indicate that our additional 3PN order terms should not be neglected for a substantial fraction of unequal mass BH binaries.

It will be useful to pursue our match computations for an extended range of the relevant parameter space. The present computations should also be extended by

invoking 1.5PN order amplitude corrections to both families of inspiral waveforms in the frame-less convention (the `LALSUITE SpinTaylorT4` and `LALSUITE SpinTaylorT2` codes do incorporate such amplitude corrections). This requires us to add certain additional 1.5PN order amplitude corrections to the usual expressions for h_{\times} and h_{+} as noted in [44]. Investigating the influence of these additional 3PN (1.5PN) order terms in phase (amplitude) while estimating the GW measurement accuracies of compact binary parameters will be interesting. It should also be worthwhile to probe the influence of these additional terms during the construction of inspiral-merger-ringdown waveforms from generic spinning BH binaries with the help of the effective-one-body approach.

Acknowledgments

We thank Riccardo Sturani for helpful discussions. We are grateful to Alejandro Bohe, Alessandra Buonanno and Guillaume Faye for useful comments on the manuscript. This is a LIGO document, LIGO-P1400178.

Appendix A. 3.5PN accurate expression for dx/dt

We list below the regular contributions to dx/dt that we employ while implementing our version of the `SpinTaylorT4` approximant. These contributions, adapted from [28], read

$$\begin{aligned}
\frac{dx}{dt} = & \frac{64}{5} \frac{c^3}{Gm} \eta x^5 \left\{ 1 + x \left[-\frac{743}{336} - \frac{11\eta}{4} \right] + x^{3/2} \left[4\pi - \frac{47}{3} s_k - \frac{25}{4} (X_1 - X_2) \sigma_k \right] \right. \\
& + x^2 \left[\left(\frac{34103}{18144} + \frac{13661}{2016} \eta + \frac{59}{18} \eta^2 \right) - \frac{1}{48} \eta \chi_1 \chi_2 \left(247(\mathbf{s}_1 \cdot \mathbf{s}_2) - 721(\mathbf{s}_1 \cdot \mathbf{k})(\mathbf{s}_2 \cdot \mathbf{k}) \right) \right. \\
& + X_1^2 \chi_1^2 \left(\frac{5}{2} (3(\mathbf{s}_1 \cdot \mathbf{k})^2 - 1) + \frac{1}{96} (7 - (\mathbf{s}_1 \cdot \mathbf{k})^2) \right) \\
& \left. \left. + X_2^2 \chi_2^2 \left(\frac{5}{2} (3(\mathbf{s}_2 \cdot \mathbf{k})^2 - 1) + \frac{1}{96} (7 - (\mathbf{s}_2 \cdot \mathbf{k})^2) \right) \right] \right. \\
& + x^{5/2} \left[-\frac{4159}{672} \pi - \frac{5861}{144} s_k - \frac{809}{84} (X_1 - X_2) \sigma_k \right. \\
& \left. + \eta \left(-\frac{189}{8} \pi + \frac{1001}{12} s_k + \frac{281}{8} (X_1 - X_2) \sigma_k \right) \right] \\
& + x^3 \left[\frac{16447322263}{139708800} + \frac{16}{3} \pi^2 - \frac{1712}{105} \gamma_E - \frac{856}{105} \ln[16x] - \frac{188}{3} \pi s_k \right. \\
& - \frac{151}{6} \pi (X_1 - X_2) \sigma_k + \eta \left(-\frac{56198689}{217728} + \frac{451}{48} \pi^2 \right) + \frac{541}{896} \eta^2 - \frac{5605}{2592} \eta^3 \left. \right] \\
& + x^{7/2} \left[\left(-\frac{4323559}{18144} + \frac{436705}{672} \eta - \frac{5575}{27} \eta^2 \right) s_k \right. \\
& + (X_1 - X_2) \left(-\frac{1195759}{18144} + \frac{257023}{1008} \eta - \frac{2903}{32} \eta^2 \right) \sigma_k \\
& \left. \left. + \pi \left(-\frac{4415}{4032} + \frac{358675}{6048} \eta + \frac{91495}{1512} \eta^2 \right) \right] \right\}, \tag{A.1}
\end{aligned}$$

where s_k and σ_k are given by

$$s_k = X_1^2 \chi_1 (\mathbf{s}_1 \cdot \mathbf{k}) + X_2^2 \chi_2 (\mathbf{s}_2 \cdot \mathbf{k}), \quad (\text{A.2a})$$

$$\sigma_k = X_2 \chi_2 (\mathbf{s}_2 \cdot \mathbf{k}) - X_1 \chi_1 (\mathbf{s}_1 \cdot \mathbf{k}). \quad (\text{A.2b})$$

We would like to stress that in the above equations we have merely replaced \mathbf{l} appearing in equation (3.16) of [28] by \mathbf{k} . This differential equation for x is also employed in the usual implementation of the SpinTaylorT4 approximant, as provided by LALSUITE SpinTaylorT4 code, while using \mathbf{l} to describe the binary orbits.

References

- [1] Sathyaprakash B S and Schutz B F 2009 *Living Rev. Relativity* **12** 2
- [2] Harry G M et al. 2010 *Class. Quant. Grav.* **27** 084006
- [3] Acernese F et al. 2015 *Class. Quantum Grav.* **32** 024001
- [4] Somiya K (LIGO Collaboration) 2012 *Class. Quant. Grav.* **29** 124007
- [5] Lueck H et al. 2006 *Class. Quantum Grav.* **23** S71–S78
- [6] Unnikrishnan C 2013 *Int. J. Mod. Phys. D* **22** 1341010
- [7] Amaro-Seoane P et al. 2012 *Class. Quant. Grav.* **29** 124016
- [8] Blanchet L 2006 *Living Rev. Relativity* **9** 4
- [9] Jaranowski P and Królak A 2012 *Living Rev. Relativity* **15** 4
- [10] Vitale S, Lynch R, Veitch J, Raymond V and Sturani R 2014 *Phys. Rev. Lett.* **112** 251101
- [11] Damour T, Iyer B R and Sathyaprakash B S 1998 *Phys. Rev. D* **57** 885
- [12] Will C M 2011 *Proc. Nat. Acad. Sci. (US)* **108** 5938
- [13] Blanchet L, Damour T and Iyer B 1995 *Phys. Rev. D* **51** 5360
- [14] Boyle M et al. 2007 *Phys. Rev. D* **76** 124038
- [15] Blanchet L, Iyer B R and Joguet B 2002 *Phys. Rev. D* **65** 064005
- [16] Blanchet L, Damour T, Esposito-Farese G and Iyer B R 2004 *Phys. Rev. Lett.* **93** 091101
- [17] Blanchet L, Faye G, Iyer B R and Sinha S, 2008 *Class. Quantum Grav.* **25** 165003
- [18] Jaranowski P and Schäfer G 2012 *Phys. Rev. D* **86** 061503
 Foffa S and Sturani R 2013 *Phys. Rev. D* **87** 064011
 Jaranowski P and Schaefer G 2013 *Phys. Rev. D* **87** 081503
 Damour T, Jaranowski P and Schäfer G 2014 *Phys. Rev. D* **89** 064058
- [19] Barker B and O’Connell R 1975 *Phys. Rev. D* **12** 329
- [20] Tulczyjew W 1959 *Acta Phys. Pol.* **18** 37
- [21] Kidder L 1995 *Phys. Rev. D* **52** 821
- [22] Apostolatos T A, Cutler C, Sussman G J and Thorne K 1994 *Phys. Rev. D* **49** 6274
- [23] Arun K G, Buonanno A, Faye G and Ochsner E 2009 *Phys. Rev. D* **79** 104023
- [24] Blanchet L, Buonanno A and Faye G 2006 *Phys. Rev. D* **74** 104034
- [25] Alvi K 2001 *Phys. Rev. D* **64** 104020
- [26] Faye G, Blanchet L and Buonanno A 2006 *Phys. Rev. D* **74** 104033
- [27] Buonanno A, Faye G and Hinderer T 2013 *Phys. Rev. D* **87** 044009
- [28] Bohe A, Marsat S and Blanchet L 2013 *Class. Quantum Grav.* **30** 135009
- [29] Marsat S, Bohe A, Faye G and Blanchet L 2013 *Class. Quantum Grav.* **30** 055007
 Bohe A, Marsat S, Faye G and Blanchet L 2013 *Class. Quantum Grav.* **30** 075017
- [30] Blanchet L arXiv:0907.3596 and references therein
- [31] Schäfer G arXiv:0910.2857 and references therein
- [32] Goldberger W D and Rothstein I Z 2006 *Phys. Rev. D* **73** 104029
- [33] Porto R 2006 *Phys. Rev. D* **73** 104031
- [34] Rafael A Porto 2010 *Class. Quantum Grav.* **27** 205001
 Levi M and Steinhoff J, arXiv:1506.05056 and references therein
- [35] Steinhoff J, Schäfer G and Hergt S 2008 *Phys. Rev. D* **77** 104018
 Steinhoff J, Hergt S and Schäfer G 2008 *Phys. Rev. D* **78** 101503
 Hergt S and Schäfer G 2008 *Phys. Rev. D* **78** 124004
 Hergt S, Steinhoff J and Schäfer G 2010 *Class. Quantum Grav.* **27** 135007
 Hartung J and Steinhoff J 2011 *Annalen der Physik* **523** 919
 Porto R A and Rothstein I Z 2008 *Phys. Rev. D* **78** 044012
 Porto R A and Rothstein I Z 2008 *Phys. Rev. D* **78** 044013
 Levi M and Steinhoff J 2014 *J. Cosmol. Astropart. Phys.* JCAP12(2014)003 and references therein

- [36] Porto R A, Ross A and Rothstein I Z 2011 *J. Cosmol. Astropart. Phys.* JCAP03(2011)009
Porto R A, Ross A and Rothstein I Z 2012 *J. Cosmol. Astropart. Phys.* JCAP09(2012)028
- [37] Buonanno A, Chen Y and Vallisneri M 2003 *Phys. Rev. D* **67** 104025
- [38] Pan Y, Buonanno A, Chen Y and Vallisneri M 2004 *Phys. Rev. D* **69** 104017
- [39] Buonanno A, Chen Y, Pan Y, Tagoshi H and Vallisneri M 2005 *Phys. Rev. D* **72** 084027
- [40] Damour T arXiv:1312.3505
- [41] Pan Y et al. 2014 *Phys. Rev. D* **89** 084006
- [42] Owen B 1996 *Phys. Rev. D* **53** 6749
- [43] <http://www.ligo.org/index.php>
- [44] Gupta A and Gopakumar A 2014 *Class. Quantum Grav.* **31** 065014
- [45] Gopakumar A and Schäfer G 2011 *Phys. Rev. D* **84** 124007
- [46] Abbott B et al. (LIGO Scientific Collaboration) 2010, Advanced LIGO anticipated sensitivity curves, Tech. Rep. LIGO-T0900288-v3 <https://dcc.ligo.org/cgi-bin/DocDB/ShowDocument?docid=2974>
- [47] Veitch J. et al. 2015 *Phys. Rev. D* **91** 042003